

Electronic standing waves on the surface of the topological insulator Bi_2Te_3

P. Rakya,¹ A. Pályi,² and J. Cserti¹

¹*Department of Physics of Complex Systems, Eötvös University,
H-1117 Budapest, Pázmány Péter sétány 1/A, Hungary*

²*Department of Materials Physics, Eötvös University,
H-1117 Budapest, Pázmány Péter sétány 1/A, Hungary*

A line defect on a metallic surface induces standing waves in the electronic local density of states (LDOS). Asymptotically far from the defect, the wave number of the LDOS oscillations at the Fermi energy is usually equal to the distance between nesting segments of the Fermi contour, and the envelope of the LDOS oscillations shows a power-law decay as moving away from the line defect. Here, we theoretically analyze the LDOS oscillations close to a line defect on the surface of the topological insulator Bi_2Te_3 , and identify an important pre-asymptotic contribution with wave number and decay characteristics markedly different from the asymptotic contributions. Wave numbers characterizing the pre-asymptotic LDOS oscillations are in good agreement with recent data from scanning tunneling microscopy experiments [Phys. Rev. Lett. **104**, 016401 (2010)].

PACS numbers: 68.37.Ef, 73.20.-r, 73.20.At

Introduction. Distinct surface-electronic properties, potentially relevant for spintronic applications, arise from the strong spin-orbit interaction in three-dimensional topological insulators (3DTIs) [1]. Although the bulk electronic structure of these materials resembles that of standard band insulators with electronic bands separated by an energy gap, the valence and conduction bands at their surfaces form a conical dispersion and touch at the center of the surface Brillouin zone. These gapless surface states lack the standard twofold spin degeneracy, are protected against backscattering, and the spin orientation of each plane-wave surface state is determined unambiguously by its momentum vector.

In the past few years, surface-sensitive experimental techniques have been utilized to explore the remarkable properties of the surface electrons in 3DTIs. The linear, Dirac cone-like electronic dispersion and deviations from that were observed in various 3DTI materials using angle-resolved photoemission spectroscopy [2–7] (ARPES), and the correlation between spin and momentum was demonstrated by the spin-resolved version of the same technique [3]. The role of electron scattering off point-like impurities and line defects on 3DTI surfaces, highly relevant for future attempts to design electronic devices based on these materials, has been studied via scanning tunneling microscopy (STM) [8–12]. In the vicinity of obstacles on the surface, characteristic standing wave patterns are formed due to the interference of initial and final scattering states [13]. These electronic standing waves contribute to the local density of states (local DOS, LDOS), therefore real-space mapping of them is possible via STM. Theories describing the standing waves on 3DTI surfaces have also been formulated recently [14–21].

A line defect has translational symmetry in the direction it stretches along, hence the electronic standing waves in its vicinity are essentially one dimensional (1D), i.e., the LDOS varies only along the axis perpendicular

to the line defect. This simple 1D character of the induced LDOS pattern implies a relatively straightforward experimental and theoretical analysis of the effect, which serves as a strong motivation to consider such arrangements. A line defect arises naturally at the edge of a step formed by an extra crystal layer on the surface [9, 11–13], hence this 1D setup is accessible experimentally.

Information on the electronic system can be extracted from the asymptotic decay exponent and wave number of LDOS oscillation around line defects. Theoretical results [12, 18–20] indicate that the LDOS oscillations on the surface of a 3DTI, asymptotically far from a line defect and within the energy range of linear dispersion, decay with the distance x from the defect as $x^{-3/2}$. This decay exponent is in contrast with the $\sim x^{-1/2}$ decay seen in a standard two-dimensional electron gas [13], and arises as a consequence of the absence of backscattering characteristic of surface electrons in 3DTIs. Recent STM data agrees with this prediction [12]. The wave vector of the asymptotic LDOS oscillations is usually equal to the distance between nesting segments of the constant-energy contour (CEC), which is the diameter of the Fermi circle in the above-mentioned case. This has been used in a recent experiment [9] to confirm the linear dispersion and to infer the Fermi velocity on the Dirac cone in Bi_2Te_3 .

For energies well above the Dirac point, the topological surface conduction band of Bi_2Te_3 is subject to strong hexagonal warping. STM data corresponding to this energy range is available [11, 12], however, the rather complex geometry of the dispersion relation has so far prevented an unambiguous theoretical interpretation of the observations. In this work, we provide a theoretical investigation of LDOS oscillations created by a line defect on the surface of Bi_2Te_3 . We describe the effect in an exact scattering-theory framework [18], yielding results that are not restricted to the spatial region asymptotically far from the defect, but hold also in the vicinity

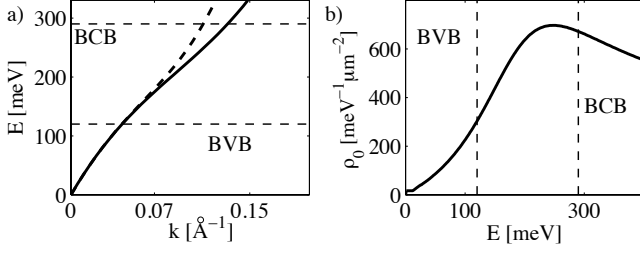


FIG. 1: (a) Surface-state conduction-band dispersion of Bi_2Te_3 along the ΓM (solid line) and ΓK (dashed line) directions of the surface Brillouin zone. (b) Surface-state conduction-band density of states of Bi_2Te_3 . [See text for band-structure parameters used in (a,b)]. The zero of energy corresponds to the Dirac point of the spectrum. Energy intervals overlapping with the bulk valence band (BVB) and bulk conduction band (BCB) are shown.

thereof. This enables us to directly compare our results with experimental data, the latter being usually taken close to the defect where features of the LDOS are most pronounced. In the energy range of strong hexagonal warping, we identify a significant pre-asymptotic contribution to the LDOS oscillations, with wave number quantitatively matching that of a recent experiment [11].

Band-structure parameters. In order to base our forthcoming calculations on an accurate surface-band dispersion, we first establish accurate values of the relevant band-structure parameters (defined below) of Bi_2Te_3 . ARPES measurements [11] indicate that the surface bands of 3DTIs with the crystal structure of Bi_2Te_3 are subject to hexagonal warping, which can be described by the envelope-function Hamiltonian [14]:

$$H(\mathbf{k}) = \gamma \mathbf{k}^2 + v_{\mathbf{k}}(k_x \sigma_y - k_y \sigma_x) + \frac{i\lambda}{2}(k_+^3 - k_-^3) \sigma_z, \quad (1)$$

where $v_{\mathbf{k}} = v_0(1 + \alpha \mathbf{k}^2)$, and $k_{\pm} = k_x \pm ik_y$. Here, $(\sigma_x, \sigma_y, \sigma_z)$ is the vector of Pauli matrices representing spin, v_0, λ, γ and α are band-structure parameters, $\mathbf{k} = (k_x, k_y)$, and k_x and k_y are momentum components along the ΓM and ΓK directions of the surface Brillouin zone, respectively. For convenience, we performed a $+\pi/2$ rotation around the z axis compared to the Hamiltonian in [14]. Energy eigenvalues of H in Eq. (1) are

$$\varepsilon_{\pm}(\mathbf{k}) = \gamma \mathbf{k}^2 \pm \sqrt{(v_{\mathbf{k}} \mathbf{k})^2 + \lambda^2 k_y^2 (k_y^2 - 3k_z^2)^2}, \quad (2)$$

where $+$ ($-$) stands for conduction (valence) band. Higher-order terms in \mathbf{k} can also be included in H [22].

Satisfactory agreement between the spectrum (2) and ARPES spectra of Bi_2Se_3 surface states [7] can be obtained by neglecting the band-structure parameters γ and α . In Bi_2Te_3 however, the experimentally determined conduction-band dispersion $\varepsilon_+(k_x, 0)$ along the ΓM direction has a sub-linear segment (see Fig. 4b in Ref. [11]), which can be described by Eq. (2) only if γ and

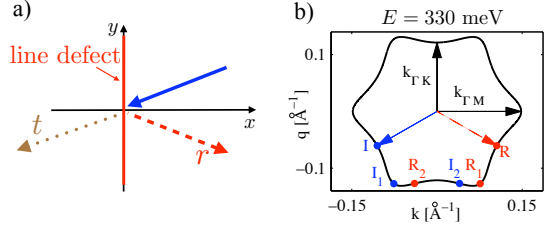


FIG. 2: (a) An incident wave from the $x > 0$ region (solid arrow) is partially reflected (dashed arrow) and transmitted (dotted arrow) at a line defect, e.g., an atomic terrace, on the surface of Bi_2Te_3 . (b) Hexagonally warped constant-energy contour in reciprocal space, corresponding to energy $E = 330$ meV above the Dirac point. Incident and reflected wave vectors from (a) are also shown.

α are finite. We find that using the band-structure parameter set $v_0 = 3.5 \text{ eV}\text{\AA}$, $\lambda = 150 \text{ eV}\text{\AA}^3$, $\alpha = 21 \text{ \AA}^2$ and $\gamma = -19.5 \text{ eV}\text{\AA}^2$, the measured dispersion relations along the ΓK and ΓM directions and the surface density of states are accurately described by H [Eq. (1)] up to 335 meV above the Dirac point. We use these parameter values throughout this paper. Fig. 1a and 1b show the theoretical dispersion curves and DOS, respectively.

Model. Our goal is to theoretically describe the oscillations in the surface-state conduction-band LDOS induced by a line defect, e.g., the edge of an atomic terrace [9–13], on the surface of Bi_2Te_3 . For the moment we assume that the defect forms a straight line that coincides with the y axis (see Fig. 2). Following [18], we model the system with the Hamiltonian $H + V$, where effect of the defect is described via the potential $V(x) = V_0 \Theta(-x)$.

Our analysis of the LDOS oscillations is based on exact energy eigenstates describing scattering of conduction-band electrons by the line defect (see Fig. 2). Therefore we first describe the scattering process of a plane wave energy eigenstate $\Phi_{k,q}(x, y)e^{iqy} = e^{iqy}e^{ikx}\chi_{k,q}$ incident from, say, the $x > 0$ side of the edge, with momentum components $k \equiv k_x$ and $q \equiv k_y$, energy E , and spin wave function $\chi_{k,q}$. Scattering at the line defect is elastic, hence the energy E is conserved. The momentum component q parallel to the defect is also conserved due to translational invariance in the y direction. The value of q determines the number of propagating waves at a given energy. E.g., in Fig. 2b, the number of propagating waves can be two (I and R) or four (I_1, I_2, R_1, R_2), depending on q .

However, the incident plane wave can be scattered into coherent superpositions of three reflected and three transmitted partial waves, for the following reasons. On the $x > 0$ side of the defect, the equation $E = \varepsilon_+(k_r, q)$ has six complex solutions [23] $k_{r,1}, \dots, k_{r,6}$ for given values of E and q , with three of the $k_{r,p}$ -s corresponding to propagating waves moving away from the defect or evanescent modes. The corresponding wave functions

$\Phi_{k_{r,p},q} = e^{iqy} e^{ik_{r,p}x} \chi(k_{r,p},q)$ ($p = 1, 2, 3$) should be included in the Ansatz of the complete scattering state. The remaining three solutions $k_{r,p}$ ($p = 4, 5, 6$) correspond to propagating waves towards the defect or diverging modes, hence they are disregarded.

These arguments, together with their generalization to transmitted waves, imply that the x -dependent component of the complete scattering wave function is

$$\psi_{k,q}^{(R)}(x) = \begin{cases} \Phi_{k,q}(x) + \sum_{p=1}^3 r_{kq,p} \alpha_{kq,p} \Phi_{k_{r,p},q}(x) & \text{if } x > 0, \\ \sum_{p=1}^3 t_{kq,p} \beta_{kq,p} \Phi_{k_{t,p},q}(x) & \text{if } x < 0, \end{cases} \quad (3)$$

where

$$\alpha_{kq,p} = \begin{cases} \sqrt{\frac{|v_{\perp,k,q}|}{|v_{\perp,k_{r,p},q}|}} & \text{if } k_{r,p} \in \mathbb{R}, \\ 1 & \text{otherwise,} \end{cases} \quad (4)$$

$$\beta_{kq,p} = \begin{cases} \sqrt{\frac{|v_{\perp,k,q}|}{|v_{\perp,k_{t,p},q}|}} & \text{if } k_{t,p} \in \mathbb{R}, \\ 1 & \text{otherwise.} \end{cases} \quad (5)$$

Here, the r -s and t -s are reflection and transmission coefficients, $v_{\perp,k,q}$ is the x -component of the group velocity of the plane wave with wave-vector components (k, q) , and the factors α and β ensure the unitarity of the scattering matrix built up from the reflection and transmission coefficients. Evanescent modes are not subject to the unitarity requirement, hence we are allowed to make the above arbitrary choice $\alpha = \beta = 1$ for partial waves with complex wave vectors. As the Hamiltonian is a third-order differential operator, partial waves at the two sides of the defect should be matched via boundary conditions ensuring their continuity as well as the continuity of their first and second derivatives. The scattering state $\psi_{k,q}^{(L)}$ of a plane wave incident from the left side ($x < 0$) of the defect can be described analogously.

The LDOS at a given energy E and position x is expressed with the exact scattering states as

$$\rho(E, x) = \frac{1}{(2\pi)^2 \hbar} \sum_{d=L,R} \int_{\Gamma_E^{(d)}} d\kappa \frac{|\psi_{k,q}^{(d)}(x)|^2}{v(k, q)}, \quad (6)$$

where $\Gamma_E^{(R)}$ [$\Gamma_E^{(L)}$] is the wave-vector contour of waves that (i) are incident from the right [left] side of the line defect, and (ii) have energy E . Note that $\Gamma_E^{(d)}$ becomes fragmented for strong hexagonal warping, e.g., in Fig. 2b, the points I_1 and I_2 belong to $\Gamma_E^{(R)}$ but R_1 and R_2 do not. The infinitesimal line segment along $\Gamma_E^{(L,R)}$ is denoted by $d\kappa$, and $v(k, q)$ is magnitude of the group velocity of the wave with momentum vector (k, q) . Using the exact scattering wave functions $\psi_{k,q}^{(d)}$, we evaluate the integral in Eq. (6) numerically. To account for the inevitable roughness of the line defect and to suppress noise due to the limited precision of the numerical integration, we

average the signal over the angular range $[-5^\circ, 5^\circ]$ of the line defect orientation with respect to the ΓK direction.

Results. In Fig. 3a, we plot the numerically computed LDOS oscillations $\delta\rho(x) \equiv \rho(x) - \rho_0$ (black points) on the $x > 0$ side of the defect, corresponding to energy $E = 330$ meV and potential step height $V_0 = -150$ meV. Motivated by recent theories using asymptotic analysis [12, 20], we fit the function $f_1(x) = A_1 \sin(2k_1 x + \varphi_1) x^{-3/2}$ via fitting parameters A_1 , k_1 , and φ_1 to the results (shown as red solid line). We also fit an exponentially decaying function $f_2(x) = A_2 \sin(2k_{\text{fit}} x + \varphi_2) e^{-x/L}$ via fitting parameters A_2 , k_{fit} , φ_2 and L (blue dashed line). The two major features of our numerical result $\delta\rho(x)$ are as follows. (i) Comparison of the three curves suggests that the decay of $\delta\rho(x)$ is better described by the exponentially decaying function $f_2(x)$ than by $f_1(x)$ having power-law decay. (ii) The wave-number value obtained from fitting $f_2(x)$ is $2k_{\text{fit}} \approx 0.178 \text{ \AA}^{-1}$.

Expectations for the wave number of the LDOS oscillations can be drawn from asymptotic analysis [12, 20]. That suggests that the wave number of an electronic standing wave at a given energy E is associated to wave vectors connecting nesting segments of the corresponding CEC [13, 14, 20], i.e., $2k_{\Gamma M} = 0.297 \text{ \AA}^{-1}$ or $k_{\text{nest}} = 0.126 \text{ \AA}^{-1}$ depicted in Fig. 3b. As the wave number $2k_{\text{fit}}$ characteristic of our data $\delta\rho(x)$ deviates significantly from $2k_{\Gamma M}$ and k_{nest} , and its decay is exponential rather than power-law, we conclude that $\delta\rho(x)$ is dominated by a pre-asymptotic contribution in the considered spatial range.

In what follows, we argue that (i) the pre-asymptotic component of the LDOS is due to the interference of incoming and reflected partial waves, i.e., the role of evanescent and transmitted partial waves is negligible, and (ii) the appearance of the characteristic wave number $2k_{\text{fit}}$ in the LDOS oscillations is due to the non-monotonic behavior of the parallel-to-defect group velocity component along the CEC. To this end, we now consider only the interference contribution of incoming and reflected propagating waves to the LDOS [Eq. (6)] on the right half plane $\rho(E, x > 0)$, rewrite it as an integral over the perpendicular-to-defect wave-vector component k , and drop the contributions from k -regions where more than one propagating reflected partial wave is allowed ($|k| < k_c$), yielding

$$\rho_r(E, x) = \frac{1}{\pi^2 \hbar} \int_{-k_{\Gamma M}}^{-k_c} dk \frac{\left(r_{k,q'} \chi_{k,q'}^\dagger \chi_{-k,q'} e^{-i2kx} + c.c. \right)}{|v_{\parallel}(E, k)|}. \quad (7)$$

Here, $q' \equiv q'(k, E)$ is the unique positive solution of $E = \varepsilon_+(k, q)$ for a fixed k and E . The integrand without the exponential factor corresponds to the Fourier transform of $\rho_r(x)$. We plot the three factors determining $\rho_r(x)$ — the magnitudes of the reflection coefficient $|r_{k,q'}|$, the spinor overlap $|\chi_{k,q'}^\dagger \chi_{-k,q'}|$, and the inverse of the parallel-to-defect group-velocity component $v_{\parallel}(k, E)$,

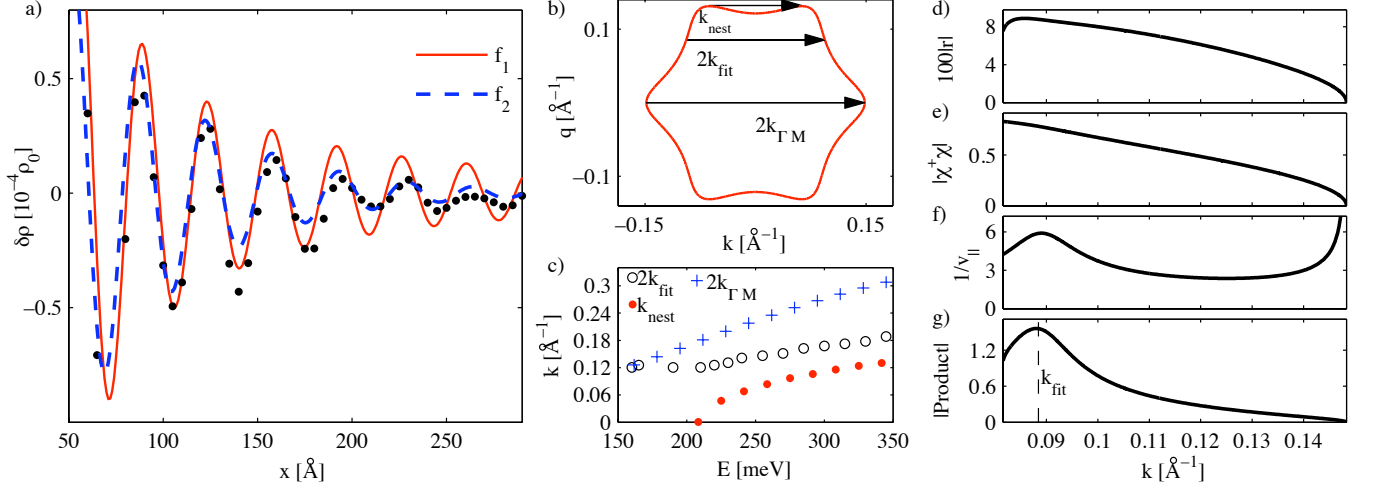


FIG. 3: (a) Position-dependent contribution $\delta\rho(E, x)$ (solid line) to the LDOS at energy $E = 330$ meV in the vicinity of a line defect (black points). Red solid and blue dashed lines are fits of the functions f_1 and f_2 (see text), respectively, to the data. $\rho_0 = 628 \text{ meV}^{-1}\mu\text{m}^{-2}$. (b) Constant-energy contour at the same energy, and relevant scattering wave vectors in reciprocal space. (c) Dominant wave number $2k_{\text{fit}}$ of $\delta\rho(E, x)$ (empty circles), and characteristic wave numbers k_{nest} (red points) and $2k_{\Gamma M}$ (blue crosses) of the constant-energy contour, as functions of energy E . (d) Magnitude of reflection amplitude $|r| \equiv |r_{k,q'}|$, (e) magnitude of spinor overlap $|\chi^\dagger\chi| \equiv |\chi_{k,q'}^\dagger\chi_{-k,q'}|$, (f) magnitude of the inverse of the parallel-to-defect group velocity component $v_{||}(k)$ (in units of 10^{-6} s/m), and (g) the product of the above three quantities (in units of 10^{-6} s/m), as functions of perpendicular-to-defect wave number component k .

— as well as their product, in Fig. 3d, e, f, and g, respectively. While Figs. 3d and e show a featureless dependence on k , Fig. 3f reveals a peak in $1/v_{||}(k)$ close to k_{fit} . Hence, a peak arises in the product of the three factors as well, shown in Fig. 3g, which explains the oscillations of the real-space data $\delta\rho(x)$ with wave number $2k_{\text{fit}}$.

We have repeated the above analysis for various energy values in the range $E \in [145 \text{ meV}, 475 \text{ meV}]$ in order to compare the characteristic wave number $2k_{\text{fit}}$ of $\delta\rho(x)$ with experimental data [11]. We plot $2k_{\text{fit}}$ as the function of energy E in Fig. 3c. For low energy $E \lesssim 170$ meV, the hexagonal warping of the CEC is weak, and our result shows $k_{\text{fit}} \approx k_{\Gamma M}$ and a decay of $\delta\rho(x) \propto x^{-3/2}$ (not shown), in agreement with the results of the asymptotic analysis [12, 20]. Between 190 meV and 345 meV above the Dirac point, our k_{fit} data in Fig. 3c differs significantly from $k_{\Gamma M}$, and the former shows good quantitative agreement with the experimental values (shown in Fig. 4b of Ref. 11). No experimental data is available below 190 meV, whereas above 345 meV, the measured data shows a pronounced kink that is not described by our model. A potential reason for that discrepancy is that the surface and bulk conduction electrons might be strongly hybridized in that high-energy range, making our surface-band model inappropriate to describe the corresponding standing-wave patterns.

At high energy $E > 200$ meV, the nesting of CEC segments connected by k_{nest} in Fig. 3b may also induce LDOS oscillations with wave number k_{nest} [12, 20]. However, in our model we find that such oscillations do not

exist, due to the exact cancellation of contributions from reflected and transmitted waves incident from the $x > 0$ and $x < 0$ regions, respectively [23].

The appearance of the LDOS contribution with wave number corresponding to the local maximum point of $1/v_{||}(k)$ is a generic feature, expected to be present in other electronic systems as well. We think that it plays a dominant role in Bi_2Te_3 because of the suppression of the other two Fourier components with wave numbers k_{nest} and $2k_{\Gamma M}$, due to the cancellation mechanism [23] and the absence of backscattering, respectively.

Summary. We theoretically described pre-asymptotic electronic LDOS oscillations in the vicinity of a line defect on the surface of Bi_2Te_3 , with wave number and decay characteristics markedly different from the asymptotic ones. The calculated energy dependence of the characteristic wave number of the LDOS oscillations is in line with STM data. In a general context, our study highlights the importance of pre-asymptotic calculation of the surface-state LDOS oscillations in the analysis and interpretation of STM experiments.

Acknowledgment. This work was supported by OTKA grants No. 75529 and No. 81492, the Marie Curie ITN project NanoCTM, the European Union and co-financed by the European Social Fund (grant no. TAMOP 4.2.1/B-09/1/KMR-2010-0003), and the Marie Curie grant CIG-293834.

Note: While completing this manuscript, we became aware of a related unpublished work [24] on electronic standing waves on 3DTI surfaces. Our results partially

overlap with those in [24]. Apart from various details of the model, the major distinctive features of our work are (i) the interpretation of the results in terms of the properties of the group velocity (Fig. 3d-g), and (ii) the quantitative agreement with the experiment [11].

Appendix A: Plane-wave states

We label the electronic plane-wave states by their energy E and the parallel-to-defect wave-number component q , which are conserved in the scattering process on the line defect (for details see the main text). Here we review a numerical method to obtain these states, which is necessary to solve the scattering problem at the edge step. For a given E and q there are six solutions of longitudinal wave vector $k_{r,p}$ ($p = 1 \dots 6$) which satisfies the characteristic equation $\det [H(k_r, q) - \hat{1}E] = 0$, where $\hat{1}$ is the 2×2 identity matrix and H is the Hamiltonian defined by Eq. (1) in the main text. Complex roots $k_{r,p}$ of the characteristic polynomial

$$\det [H - \hat{1}E] = \sum_{k=0}^6 a(E, q) k_r^k \quad (8)$$

are equal to eigenvalues of the companion matrix [25] of this polynomial, hence we find the roots $k_{r,p}$ by numerically diagonalizing the companion matrix. Then, the spinor component χ of the corresponding plane wave $\Phi_{k_{r,p},q}(x, y) = e^{iqy} e^{ik_{r,p}x} \chi(k_{r,p}, q)$ can be numerically computed from the eigenvalues problem

$$H(k_{r,p})\chi(k_{r,p}, q) = E\chi(k_{r,p}, q) \quad (9)$$

for $p = 1, \dots, 6$.

Appendix B: Cancellation of reflected and transmitted waves in LDOS oscillation

In this section we show the exact cancellation of reflected and transmitted waves in LDOS oscillation for wave number k_{nest} connecting nesting segments on the constant energy contour (see Fig. 3b in the main text). Transmitted wave from the left side ($x < 0$) to the right side of the line defect ($x > 0$) leads to oscillation in the LDOS at $x > 0$ only in case there are at least two transmitted propagating states on the right. We assume in the relevant regime of transverse wave number q two incident states on the right and one incident state on the left side of the line defect. We denote the wave numbers of the two incident electronic states on the right side with k_1 and k_2 , while the incident wave number on the left side is labeled with \tilde{k} . Each incident electronic state on the right is reflected into two propagating (and one evanescent) states with reflection amplitudes $r_{k_1q,p}$ and $r_{k_2q,p}$

($p = 1, 2$). The incident state on the left is transmitted into two propagating states on the right with transmission amplitudes $t_{\tilde{k}q,p}$ ($p = 1, 2$). The two reflected states labeled with $p = 1$ and $p = 2$ are connected with stationary wave vector k_{nest} (see Fig. 3b). From Eq. (3) follows that the oscillatory part of the integrand in Eq. (7) with wave number k_{nest} is then proportional to:

$$\text{Re} \left[2 \left(r_{k_1q,1}^* r_{k_1q,2} + r_{k_2q,1}^* r_{k_2q,2} + t_{\tilde{k}q,1}^* t_{\tilde{k}q,2} \right) e^{ik_{\text{nest}}x} \right]. \quad (10)$$

On the other hand, the quantity in the inner brackets vanishes due to the unitarity of the scattering matrix. Therefore, the components of the LDOS oscillation with nesting vector k_{nest} are canceled due to the destructive interference of the reflected and transmitted waves. Note that the same statement can be made if there are two incident states on the left side of the line defect.

-
- [1] M. Z. Hasan and C. L. Kane, Rev. Mod. Phys. **82**, 3045 (2010).
 - [2] D. Hsieh, D. Qian, L. Wray, Y. Xia, Y. S. Hor, R. J. Cava and M. Z. Hasan, Nature **452**, 970 (2008).
 - [3] D. Hsieh *et al.*, Science **323**, 919 (2009).
 - [4] Y. Xia *et al.*, Nat. Phys. **5**, 398 (2009).
 - [5] Y. L. Chen *et al.*, Science **325**, 178 (2009).
 - [6] D. Hsieh *et al.*, Phys. Rev. Lett. **103**, 146401 (2009).
 - [7] K. Kuroda, M. Arita, K. Miyamoto, M. Ye, J. Jiang, A. Kimura, E. E. Krasovskii, E. V. Chulkov, H. Iwasawa, T. Okuda, K. Shimada, Y. Ueda, H. Namatame and M. Taniguchi Phys. Rev. Lett. **105**, 076802 (2010).
 - [8] P. Roushan, J. Seo, C. V. Parker, Y. S. Hor, D. Hsieh, D. Qian, A. Richardella, M. Z. Hasan, R. J. Cava and A. Yazdani, Nature **460**, 1106 (2009).
 - [9] T. Zhang *et al.*, Phys. Rev. Lett. **103**, 266803 (2009).
 - [10] J. Seo, P. Roushan, H. Beidenkopf, Y. S. Hor, R. J. Cava and A. Yazdani, Nature **466**, 343 (2010).
 - [11] Z. Alpichshev, J. G. Analytis, J.-H. Chu, I. R. Fisher, Y. L. Chen, Z. X. Shen, A. Fang and A. Kapitulnik, Phys. Rev. Lett. **104**, 016401 (2010).
 - [12] J. Wang, W. Li, P. Cheng, C. Song, T. Zhang, P. Deng, X. Chen, X. Ma, K. He, J.-F. Jia, Q.-K. Xue, B.-F. Zhu, arXiv:1105.1957 (unpublished).
 - [13] M. F. Crommie, C. P. Lutz and D. M. Eigler, Nature **363**, 524 (1993).
 - [14] L. Fu, Phys. Rev. Lett. **103**, 266801 (2010).
 - [15] W.-C. Lee, C. Wu, D. P. Arovas and S.-C. Zhang, Phys. Rev. B **80**, 245439 (2009).
 - [16] H. M. Guo and M. Franz, Phys. Rev. B **81**, 041102(R) (2010).
 - [17] Q.-H. Wang, D. Wang and F.-C. Zhang, Phys. Rev. B **81**, 035104 (2010).
 - [18] X. Zhou, C. Fang, W.-F. Tsai, and J. Hu, Phys. Rev. B **80**, 245317 (2009).
 - [19] R. R. Biswas and A. V. Balatsky, Phys. Rev. B **83**, 075439 (2011).
 - [20] R. R. Biswas and A. V. Balatsky, arXiv:1005.4780 (unpublished).
 - [21] Q. Liu, arXiv:1108.6051 (unpublished).

- [22] S. Basak, H. Lin, L. A. Wray, S.-Y. Xu, L. Fu, M. Z. Hasan, and A. Bansil, Phys. Rev. B **84**, 121401(R) (2011).
- [23] See Appendix for more details.
- [24] D. Zhang and C. S. Ting, arXiv:1110.3722 (unpublished).
- [25] R. A. Horn and C. R. Johnson, *Matrix Analysis* (Cambridge University Press, 1985).